CrossMark

Effect of sulfur concentration on the properties of tin disulfide thin films by nebulizer spray pyrolysis technique

A. M. S. Arulanantham[1] · S. Valanarasu[1] · K. Jeyadheepan[2] · A. Kathalingam[3] ·
I. Kulandaisamy[1]

Abstract Influence of sulfur concentration variation on the physical and chemical properties of nebulizer spray pyrolysis deposited SnS_2 thin films are investigated. The SnS_2 thin films were coated onto glass substrate at 325 °C by changing sulfur concentration as 0.8, 0.9 and 1.0 M. Sulfur concentration dependent micro-structural, surface morphological, optical and electrical characteristics of the films were studied using X-ray diffraction, Raman analysis, scanning electron microscope, atomic force microscope, UV–Vis spectroscopy, photoluminescence spectroscopy and Hall Effect measurement, respectively. X-ray diffraction measurements demonstrated the growth of crystalline SnS_2 films of hexagonal structure with preferred orientation along (002) plane. Scanning electron microscopic study revealed needle shape and basket knitting shape morphology of deposited films. The films showed direct band gap ranging from 2.02 to 2.18 eV depending on sulfur concentration. Hall measurement revealed the conductivity and mobility ranging from 10^{-3} to 10^{-2} (1/Ω-cm) and 1.4×10^2 to 3.01×10^2 (cm^2/V s) respectively.

✉ S. Valanarasu
valanroyal@gmail.com

1   PG & Research Department of Physics, Arul Anandar College, Karumathur 625 514, India

2   Multifunctional Materials & Devices Lab, Anusandhan Kendra – II, School of Electrical and Electronics Engineering, SASTRA University, Tirumalaisamudram, Thanjavur 613 401, India

3   Millimeter-Wave Innovation Technology Research Center (MINT), Dongguk University, Seoul 04620, Republic of Korea

1 Introduction

The demand of energy is continuously increasing worldwide, and as a result, the environmental degradation is also increasing. In order to avoid problems encountered in the use of fossil energy, an intensive research activity is being carried out in solar energy conversion process. Thin film solar cells have engrossed an increasing interest with the aim of reducing the cost to make it energy efficient [1]. In the thin film based solar cells, numerous chalcogenide semiconductors such as SnS, SnSe, GeS, and GeSe are realized as the potential materials for solar photovoltaic conversion [2]. Due to their enhanced optoelectronic properties, these twofold compounds are conceivably used in optoelectronic and photoconductive devices [3, 4]. Tin chalcogenides, IV–VI compound semiconductors, have been attracting extensive importance in the field of photovoltaic energy conversion [5, 6]. Tin disulfide (SnS_2) is a PbI_2-like layered material, in which the tin atoms are positioned in octahedral sites of the hexagonal structure, in between two hexagonally close packed sulfur slabs, to form a sandwich structure [3]. As a layered material, the SnS_2 has interesting properties to be useful for thin film solar cells. Its band gap energy is varying in a wide range between 0.8 and 2.88 eV [7, 8]. The constituent elements which form SnS_2 are cheap and non-toxic. It can be used as an active window layer in the place of CdS. Thin films of SnS_2 can be formed as a single phase material by vapor phase methods [9]. It has been studied using variety of techniques such as chemical deposition [10], spray pyrolysis [11], chemical vapor transport [12], SILAR [3, 13], ultrasonic spray pyrolysis [1], electron beam evaporation [14], and electro-deposition [15]. Each technique has its own advantage and disadvantage to produce quality thin films. Though there are a variety of techniques, researchers are more interested in a method which is more economical,

expedient for large area deposition of highly smooth and uniform films well adhered to the substrates. In this way, nebulizer spray pyrolysis (NSP) technique is simple and inexpensive method compared to other methods. The nebulizer spray method was adopted to deposit SnS_2 thin films at 325 °C temperature in this work. Sulfur concentration and other deposition parameters were optimized to get high-quality films. The main aim was is to prepare SnS_2 thin films by varying sulfur molarities as 0.8, 0.9, and 1.0 M using nebulizer spray pyrolysis (NSP) technique and to characterize them for the thin films solar cells application.

2 Experimental

2.1 Materials

In the typical synthesis procedure, analytical grade tin (IV) chloride ($SnCl_4$) and thiourea were used as source materials for Sn and S ion respectively. Excess concentration of thiourea was taken to compensate for the sulfur loss during deposition process [16] of SnS_2 layers.

2.2 Method

Figure 1 shows the schematic block diagram of nebulizer spray pyrolysis (NSP) experimental set-up, which comprises a purified ambient air compressor and pressurized air storage tank with air flow regulator, nebulizer kit with a L-shaped mist guiding tube which is a glass tube of 50 mm inner diameter and a controlled electrical heating furnace. The compressed air is allowed to flow through the nebulizer having the precursor solution. Nebulizer, having 0.5 mm of nozzle diameter changes the precursor solution into very small droplets due to the double collision process of the compressed air with the precursor solution.

1. Compressor 2. Air flow controller 3. Nebulizer 4. Carrier tube 5. Furnace
6. Thermocuple 7. Temperature controller 8. Exhaust
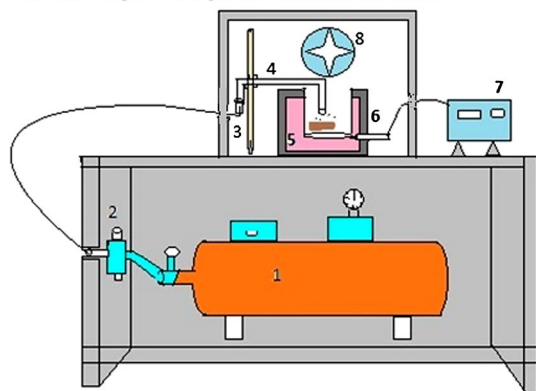
Fig. 1 Schematic diagram of NSP Technique

When the aerosol touches the heated glass substrates, evaporation of solvent takes place from the outer surface of the droplets due to the diffusion of heat in to the droplets, followed by a heterogeneous reaction [17], which leads to the formation of thin films on the glass substrates.

Parameters used for the deposition of tin disulfide thin films are;

Solvent	3:1 ratio of isopropyl alcohol and water
Tin molarity (Sn)	0.5 M
Sulfur molarity (S)	0.8–1.0 M
Substrate temperature	325 °C
Volume of the solution	5 ml

Glass substrate of about 25×25 mm area was cleaned by liquid detergent and soaked in newly prepared hot chromic acid for 1 h and then systematically cleaned using ultrasound in the double-distilled water and acetone medium. Finally, the glass substrate was dried using hot air drier before the deposition of SnS_2 films. In the present work, the solvent used was isopropyl alcohol and water with 3:1 ratio, in which the isopropyl alcohol was taken as the major content of the solvent to avoid the oxidation of the SnS_2 thin films during deposition and to avoid the formation of tin oxides.
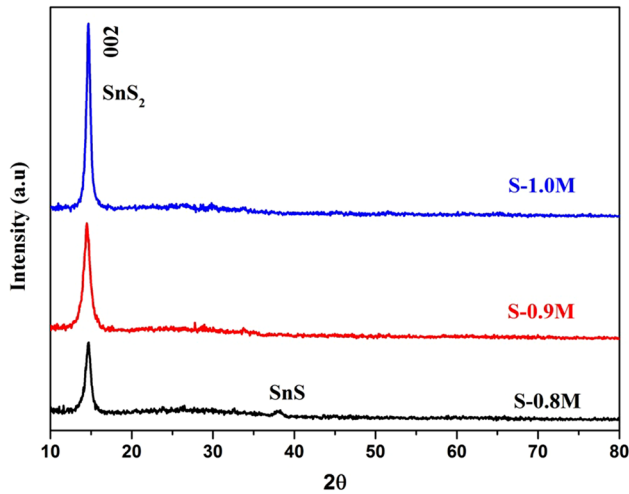
2.3 Characterization

X-ray diffraction (XRD) study was used to characterize the grown SnS_2 films. Structural properties such as crystalline phase, grain size, dislocation density, strain etc. were analyzed using X-ray diffraction studies. Optical transmittance of the film was obtained using UV-Vis-NIR double beam spectrometer. The morphological examination was done using scanning electron microscope (FEI Quanta 200 ESEM) and resistivity measurement of the films was carried out with the help of Keithley 2450 source meter unit (SMU).

3 Result and discussion

3.1 Structural characterization

Figure 2 shows the XRD patterns of nebulizer sprayed SnS_2 films coated with sulfur concentrations of 0.8, 0.9 and 1.0 M at 325 °C. As seen in Fig. 2, an increase in sulfur concentration has increased the crystallinity and the preferential orientation along (0 0 2) plane of hexagonal structure. The 2θ values observed at 14.63°, 14.68°, and 14.74° for sulfur concentrations of 0.8, 0.9 and 1.0 M respectively, are closely matched to the results of Panda et al. [18] with 2θ value of broad peak at 14.88° for dip coated SnS_2 thin films and Vijayakumar et al. [19] with 2θ value of broad peak at

Fig. 2 XRD patterns of SnS$_2$ thin films prepared different sulfur molarity for S-1.0M, S-0.9M, and S-0.8M

Table 1 Results of the calculation of the texture pole density (Pi) and orientation factor (f)

Sulfur molar concentration (M)	h k l	Pole density (p_i)	Orientation factor (f)
0.8	0 0 2	1.7	0.52
0.9	0 0 2	2.1	0.61
1.0	0 0 2	2.2	0.68

14.45° for spray deposited SnS$_2$ thin film. Whereas, sulfur concentration 0.8 M shows an extra peak at 38.17° which attributes to mixed phases of SnS$_2$ and SnS as reported by Messaoudi et al. [1]. It is reported that the SnO$_2$ phases can also be formed during the pyrolysis, if the substrate temperature is kept above 350 °C [5]. In the present work, the substrate temperature is kept constantly at 325 °C, by which the formation of oxide phases is avoided. The XRD results also elucidate that the prepared SnS$_2$ thin films are not having any peaks correspond to the oxides of tin. It is also noticed from Fig. 2 that the mixed phase found, for sulfur concentration 0.8 M, is disappeared on increasing the sulfur concentration. These results indicate that precursor's molar ratio controls the phase purity and phase composition of nebulizer sprayed thin films.

Texture quality of prepared SnS$_2$ thin films was calculated using the Harris equation [20, 21]. The pole density (P$_i$) was calculated by using the expression given in equation (1) [21].

$$p_i = \frac{(I_i/I_{oi})}{\frac{1}{N} \sum (I_i/I_{oi})} \tag{1}$$

where I$_{oi}$ and I$_i$ are the total intensities of reference and diffraction peaks of the film, respectively and N is number of peaks present in the XRD pattern.

Orientation factor was calculated using the Eq. (2) [21, 22]

$$f = \sqrt{\frac{1}{N} \sum_{i-1}^{N} (P_i - 1)^2} \tag{2}$$

Calculations by inverse pole figures method reveals texture growth along (0 0 2) plane for SnS$_2$ films. The direction of texture growth coincides with the growth direction of most crystallites of SnS$_2$ thin films [21, 23]. Calculated orientation factors of the films are as shown in Table 1, it shows high values of texture growth. Samples deposited at 1.0 M concentration shows orientation factor of 0.68; while decreased sulfur concentration 0.9 M leads to a decrease in orientation factor to 0.61. For further decrease of sulfur concentration to 0.8 M, the growth texture of the layers decreased slightly to 0.52; this trend of change is similar to the results reported by Opanasyuk et al. [22].

Average crystallite size of SnS$_2$ films was determined from predominant XRD peak (002) using Scherrer Eq. (3) [24],

$$D = \frac{k\lambda}{\beta \cos\theta} \tag{3}$$

where k = 0.9 the numerical shape factor which is a constant, D is crystallite size, λ is wavelength of incident radiation, β is the FWHM in radians, and θ is Bragg angle taken in radians. The crystallite size is increased with sulfur concentration, which is evident from the decrease in full width at half maximum (FWHM) value of (0 0 2) XRD peak [24].

Dislocation density (δ) was calculated from crystallite size using Eq. (4) [25, 26].

$$\delta = \frac{1}{D^2} \tag{4}$$

Also strain (ε) of tin sulfide (SnS$_2$) film was calculated using the Eq. (5) [26, 27]

$$\varepsilon = \frac{\beta \times \cos\theta}{4} \tag{5}$$

The variation of dislocation density of SnS$_2$ thin films with various sulfur molar concentration is given in Table 2. It shows decrease of dislocation density and strain for the increase of sulfur molarity from 0.8 to 1.0 M. This can be attributed to the improvement in crystallinity due to regular arrangements of atoms in crystal lattice at higher sulfur concentration [25].

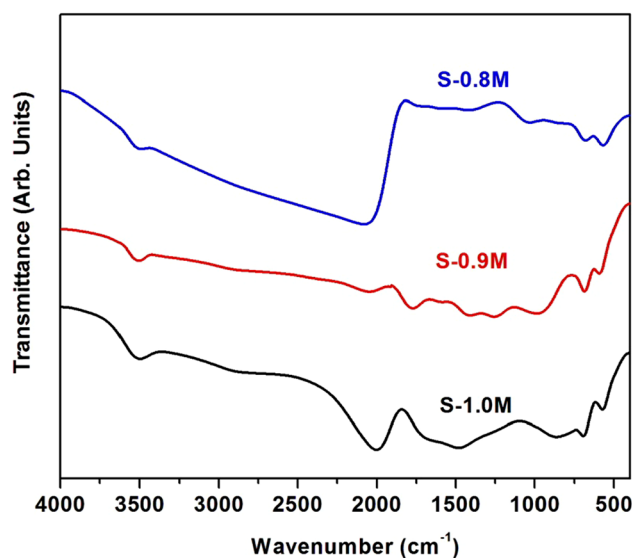**Table 2** Structural parameters of deposited SnS_2 thin films in various sulfur concentration

Sulfur molar concentration (M)	Crystallite size (nm)	Dislocation density ($\delta \times 10^{15}$ lines. m^{-2})	Strain($\varepsilon \times 10^{-3}$ lines^{-2}. m^{-4})
0.8	23	1.84	1.1
0.9	27	1.35	1.0
1.0	40	0.6	0.6

3.2 Raman analysis

Raman spectra of SnS_2 thin films obtained in the wavelength range 50–1000 cm^{-1} at room temperature are shown in Fig. 3. All the films exhibited Raman peaks correspond to SnS_2. The intense peak observed at 312 cm^{-1} for all the films is assigned to the A_{1g} mode of SnS_2 [28] structure. Intensity of the Raman peak 312 cm^{-1} is increased for the increase of sulfur concentration from 0.8 to 1.0 M and the FWHM of the decreased with the increase sulfur concentration. This attributes to the improvement in crystallinity of the film [18]. Appearance of only A_{1g} mode confirms growth of single-phase as indicated by XRD study [21]. Low FWHM value of dominating A_{1g} mode Raman peak indicates high structural quality of the deposited films.

3.3 FTIR analysis of SnS_2 thin films

FTIR spectra obtained for SnS_2 thin films in the wave number range 400–4000 cm^{-1} are as shown in Fig. 4. It reveals typical absorbance at 3506, 2040, 682 and 573 cm^{-1} proving the presence of hydroxyl groups, C=C and Sn–S groups in all the three samples. The weak absorption peak displayed at 3506 cm^{-1} is attributed to the O–H stretching vibration
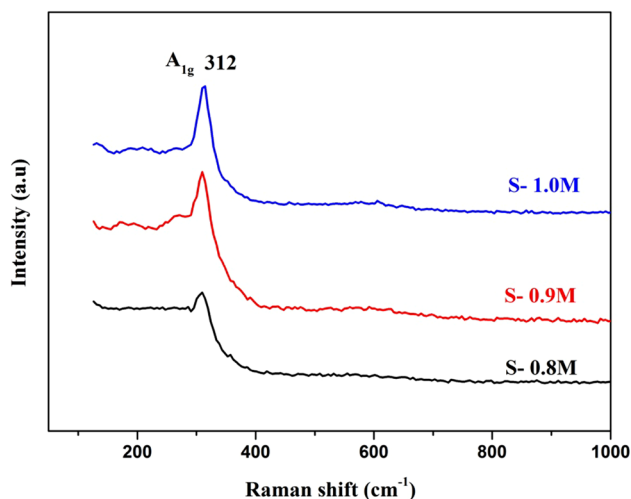

Fig. 4 FTIR Spectra of SnS_2 thin films deposited with various sulfur concentration

of surface adsorbed water in the thin film samples [29]. Also, the presence of water is confirmed by its bending vibration observed at 1445 cm^{-1}, as reported with a nearest absorption peak by Mani et al. [30]. The small absorption peaks observed at 573 and 682 cm^{-1} are probably due to the stretching vibration of Sn–S bond [30]. The peak appeared around 2040 cm^{-1} could be ascribed to C=C vibration which may be due to the organic contamination from the solvent used [30, 31]. These characteristic peaks of SnS_2 in FT-IR analysis are supported by XRD result confirming the presence of SnS_2 thin films.

3.4 Morphological analysis of SnS_2 thin films

SEM images of SnS_2 thin films coated using different sulfur concentration from 0.8 to 1.0 M are shown in Fig. 5. Pinholes and cracks free uniform deposition of films are observed which clearly display the molar concentration dependent variation of surface morphology. As seen from Fig. 5a, the concentration 0.8 M has given needle-shaped grains without cracks [32]. Figure 5b, the SEM image of the film deposited for 0.9 M concentration of sulfur, displays many pores with rod-shaped grains [33]. Films coated with 1.0 M sulfur concentration have basket knitting shape arrangement of rod-shaped grains with many pores which can be inferred from Fig. 5c. It is inferred that the grain size is increased with the increase of sulfur concentration. Increased sulfur concentration promotes grain growth and sintering. The porous nature of SnS thin films renders an increased surface area, which is beneficial for the excitonic hybrid inorganic–organic solar cells [34].


Fig. 3 Raman spectra of SnS_2 thin films at different sulfur molarities
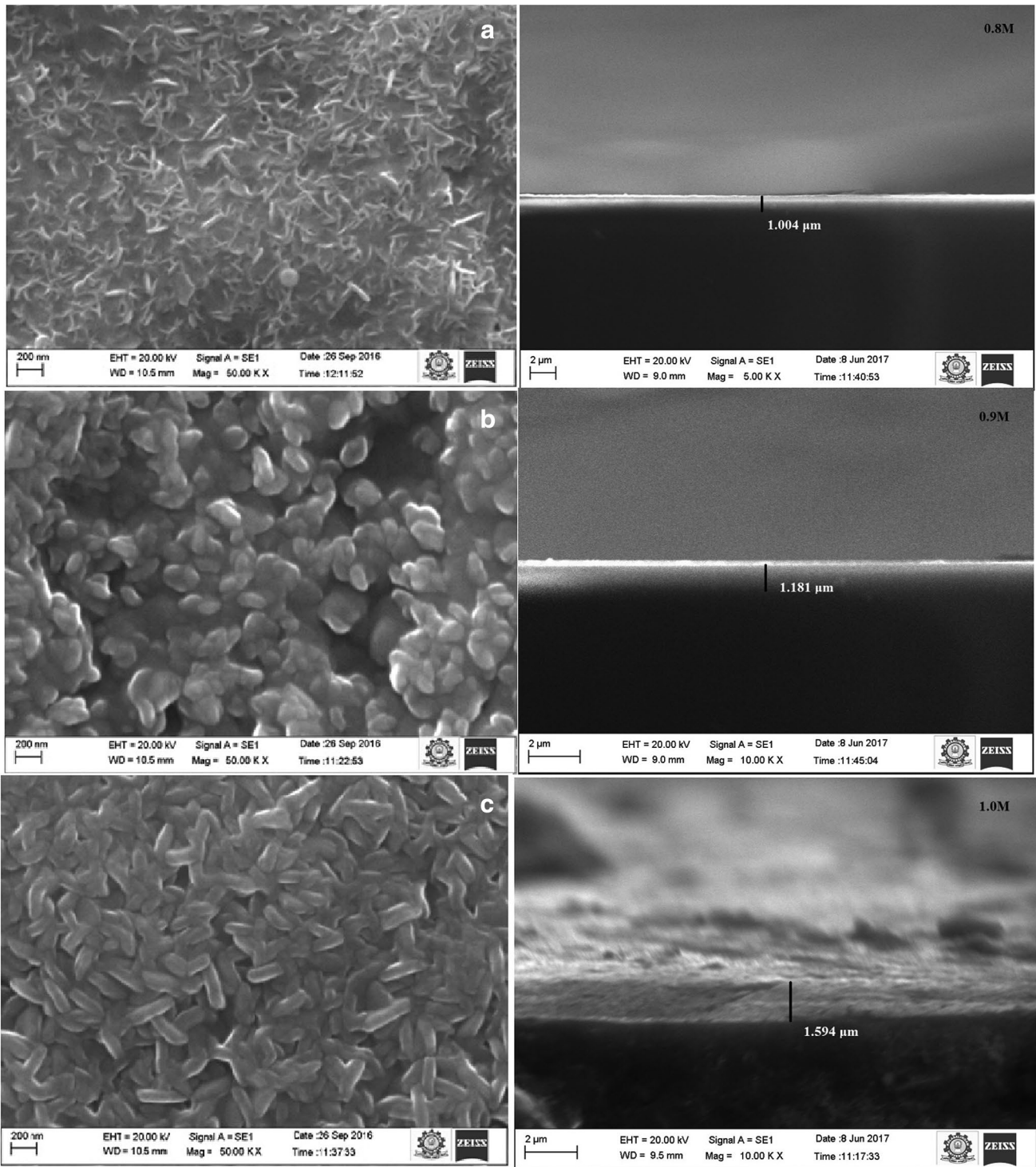
Fig. 5 SEM and cross-sectional SEM image of SnS$_2$ films prepared different sulfur molarities are **a** 0.8 M, **b** 0.9 M, and **c** 1.0 M

The cross-sectional SEM images of SnS$_2$ films deposited at different sulfur concentrations are also shown in Fig. 5. It can be inferred from the cross-sectional SEM that the prepared SnS$_2$ films are almost pinhole free and the thickness of the films are increased from 1 to 1.5 µm with the increase of sulfur concentration from 0.8 to 1.0 M.

3.5 Compositional analysis

Representative EDAX spectra of SnS_2 films deposited at various sulfur concentration are shown in Fig. 6a–c. The EDAX spectra confirm the presence of tin and sulfur in all the films. Atomic percentages of elements in various films are shown in Table 3. The non-stoichiometry of SnS_2 observed may be due to either Sn^{2+} vacancies or elemental tin creating deep acceptor energy states with wide activation energy in
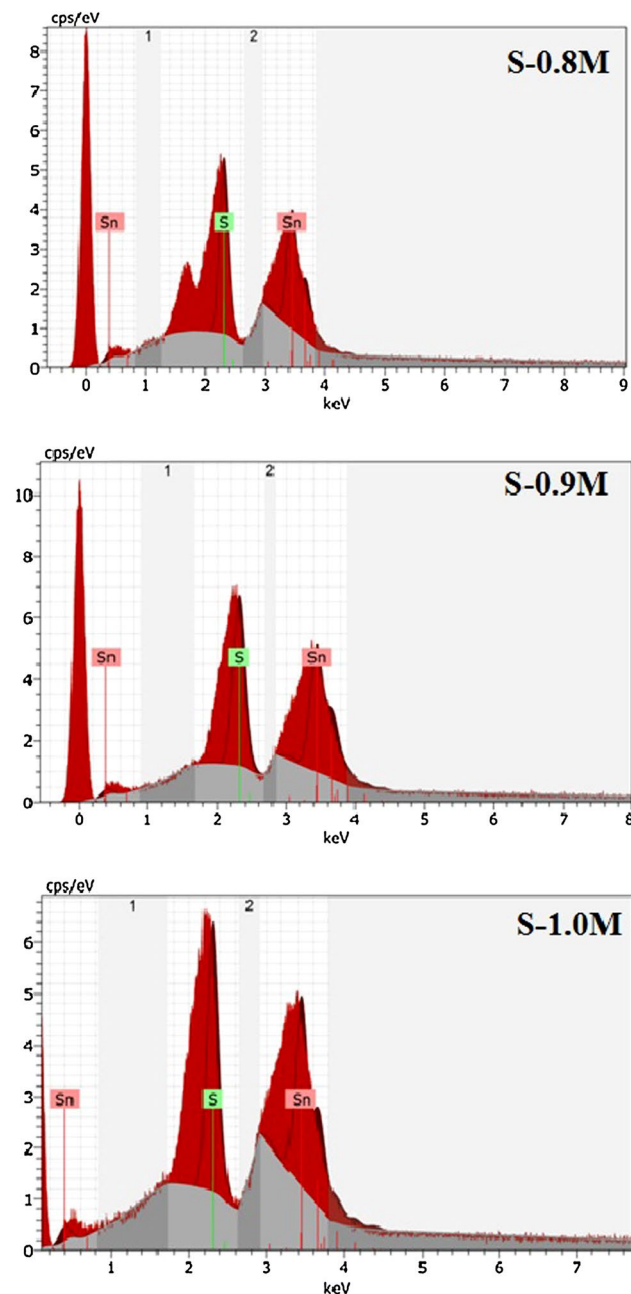
Table 3 Composition of SnS_2 films deposited at various sulfur concentration obtained from EDAX analysis

Sulfur molar concentration (M)	Sn (%)	S (%)	S/Sn
0.8	37.92	62.08	1.6
0.9	30.53	69.47	2.2
1.0	28.57	71.43	2.5

the range 0.2 and 0.45 eV, where both are depending on the coating technique [35].
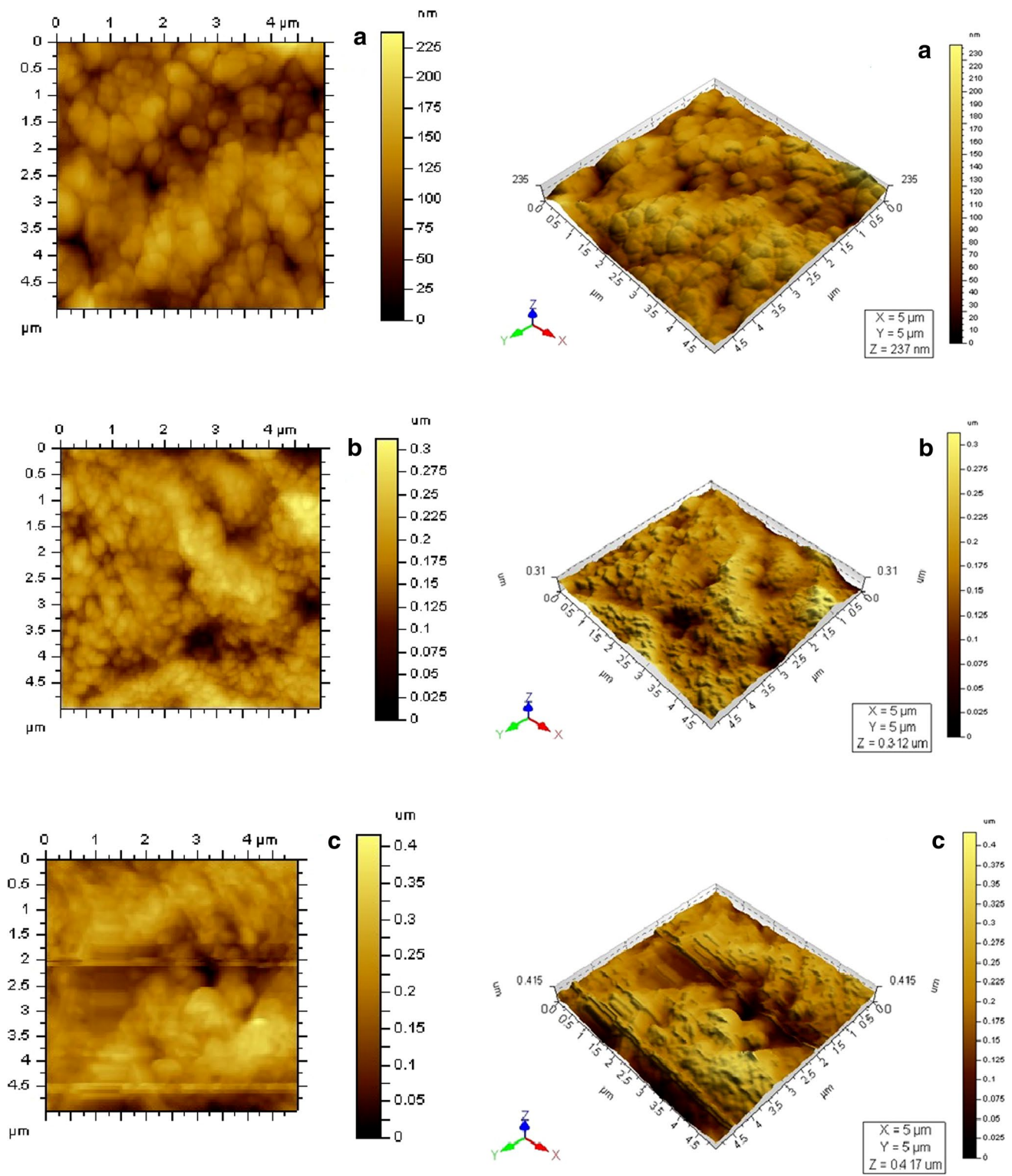
3.6 AFM studies of SnS_2 films

Surface topography of SnS_2 thin films has been recorded using atomic force microscopy (AFM) system. 2D and 3D AFM images (5.0 μm × 5.0 μm) of SnS_2 thin films with various sulfur concentration are presented in Fig. 7. These results confirm that root-mean-square (RMS) surface roughness and the average size of the particles distributed over the surface depend on sulfur content. The 2D images indicate island-type formation of grown SnS_2 films, which are the agglomeration of smaller grains (Volmer–Weber growth mechanism) [36]. Increase of sulfur concentration from 0.8 to 1.0 M reduced roughness indicating uniform coating of the film. The RMS roughness value of SnS_2 film for 0.8 M concentration is about 60 nm, and it is decreased to 28 nm for 1.0 M sulfur concentration. This similar report of roughness value decrease with sulfur concentration has been reported in literature [14]. Pore size and density of the films are also decreased with sulfur concentration increase.

3.7 Optical analysis of tin disulfide (SnS_2) thin films

Figures 8 and 9 show transmittance and absorbance spectra of SnS_2 films in the range of 400–1000 nm for different sulfur molarity. It is perceived that there is a significant increase in transmittance for an increase in sulfur concentration, which attributes increased absorption of the films at decreased sulfur concentration. Optical band gap (E_g) of SnS_2 films was determined from Tauc formula [26].

$$(\alpha h\nu)^2 = A(h\nu - E_g) \qquad (6)$$

where α is the absorption coefficient, A is a constant independent on photon energy ($h\nu$), and h is the Planck's constant. The plot of $(\alpha h\nu)^2$ versus ($h\nu$) for the SnS_2 film is shown in Fig. 10. E_g was determined by extrapolating the linear portion of the $(\alpha h\nu)^2$ versus ($h\nu$) plot to $\alpha = 0$ and the bandgap values are tabulated in Table 4. The optical band gap of the films is varying with respect to the sulfur ratio which may lead to the change in the entire energy band
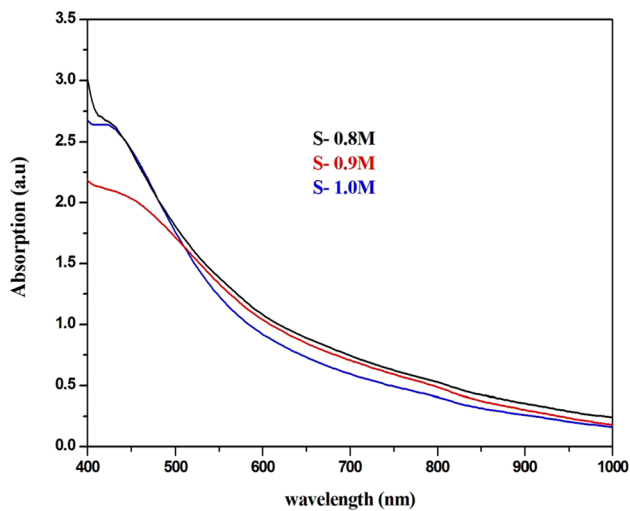

Fig. 6 EDX spectrums of SnS_2 films prepared different sulfur molarities are **a** 0.8 M, **b** 0.9 M, and **c** 1.0 M

Fig. 7 Atomic force microscopy (AFM) images of SnS$_2$ films deposited at different sulfur concentrations **a** 1.0 M, **b** 0.9 M and **c** 0.8 M
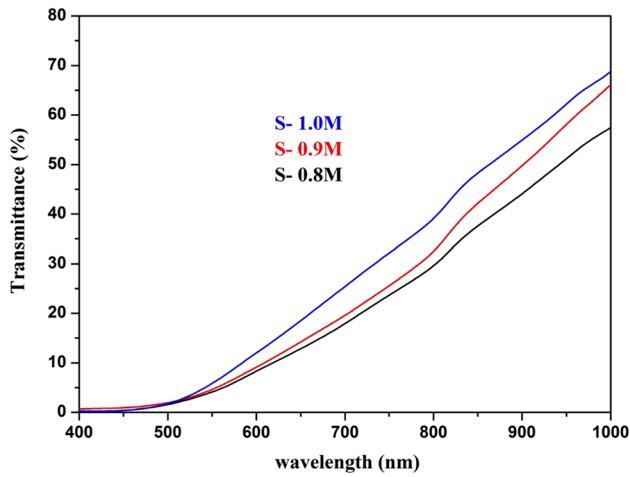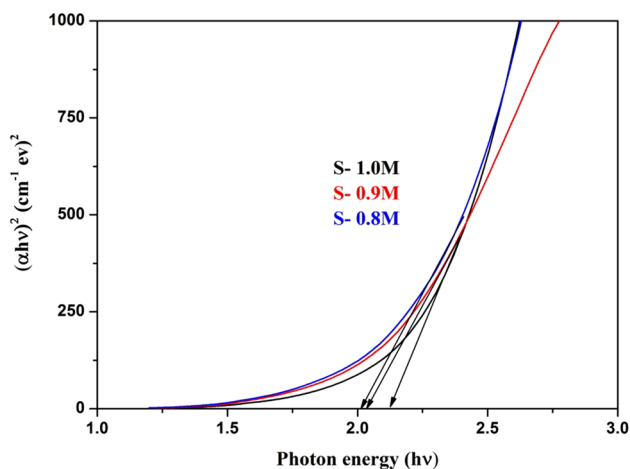
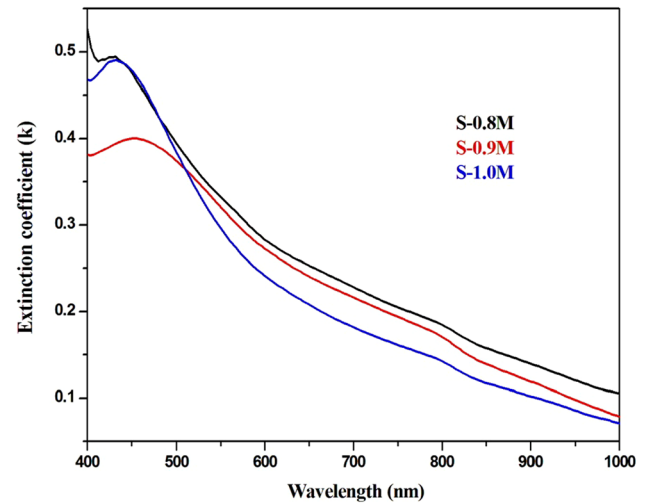**Fig. 8** Transmittance versus wavelength spectra of SnS_2 films

Fig. 9 Absorption versus wavelength spectra of SnS_2 films

Fig. 10 Plots of $(\alpha h\nu)^2$ versus photon energy, $h\nu$

Table 4 Band gap value of deposited SnS_2 thin films

Sulfur molar concentration (M)	Energy gap (E_g) eV
0.8	2.02
0.9	2.09
1.0	2.18

Fig. 11 Extinction coefficient versus wavelength spectra of SnS_2 films

structure [37] of the SnS_2 material. The estimated optical energy gap of SnS_2 films agree with the results reported by Yassin et al. [38]. Extinction coefficient of the films were calculated using the relation, [39]

$$k = \frac{\alpha\lambda}{4\pi} \tag{7}$$

Variation of extinction coefficient with wavelength for SnS_2 films deposited at various sulfur concentration is shown in Fig. 11. Extinction coefficient is increased initially due to increased absorption. For further increase of wavelength, the extinction co-efficient is decreased, which is associated to the increasing transmittance and decreasing absorption coefficient [39].

The refractive index (n), an optical constant was calculated for the coated thin films using the following equation [40].

$$n = \left(\frac{4R}{(R-1)^2} - k^2 \right)^{1/2} - \frac{R+1}{R-1} \tag{8}$$

The variation of refractive index with wavelength, obtained for SnS_2 films prepared with different sulfur concentrations (0.8, 0.9, and 1.0 M) at 325 °C is as shown in
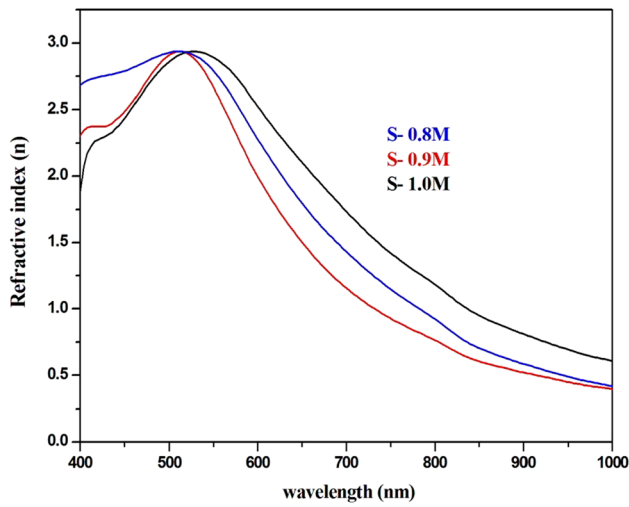
Fig. 12 Refractive index (n) versus wavelength spectra of SnS_2 films
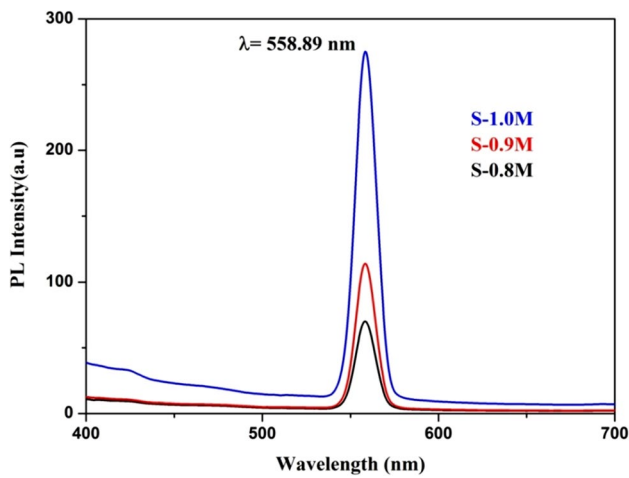

Fig. 13 PL spectrum of tin disulfide (SnS_2) thin films deposited at different sulfur concentration

Fig. 12. Refractive index is increased from 2.49 to 2.8 for the increase of sulfur concentration. This increase of refractive index can be due to the increase of molar concentration which can make SnS_2 more denser (increasing the packing density) which in turn decrease the propagation velocity of light through them. This behavior can also be explained

based on the fact that the refractive index of bulk material is higher than the thin film. As the thickness increases at increased concentration, refractive index increases and according to inverse relation between refractive index and energy gap the band gap is increased [40].

3.8 Photoluminescence studies

Photoluminescence (PL) measurement of SnS_2 thin films was performed with the excitation wavelength of 300 nm and that is plotted in Fig. 13. The PL spectra recorded at room temperature consist of one strong peak located at the wavelength of about 558.89 nm which can be ascribed to the near band edge emission (NBE) results from the recombination of free or bound excitons [41]. No change in peak position is observed for the change of sulfur concentration. The NBE peak observed at about 558 nm, corresponding to energy 2.24 eV is slightly higher than the band gap calculated from UV–Vis analysis. The increase in the intensity of the NBE peak with the sulfur concentration is due to the enhancement of radiative recombination in luminescent process [42, 43].

4 Electrical studies

The electrical characterization is important since it enables us to measure resistivity, mobility and carrier concentration giving insight into the mechanism of conductivity in semiconductors. The measured electrical properties, for the samples, are summarized in Table 5. It is observed that the resistivity is decreased with the increase in S ion concentration and it is ranged between, 6.09×10^2 to 0.11×10^2 Ω-cm. The film deposited with 1.0 M concentration shows very low resistivity values due to the higher crystalline size, as seen in Table 2. Also, Hall mobility has increased to a maximum value 8.27×10^2 cm²/V s for the increase of concentration from 0.8 to 0.9 M then decreased rapidly for the further increase to 1.0 M concentration. At low concentration, the crystallites cannot grow amply large, so that the inter crystallite regions are wide to offer high resistivity to the mobility of charge carriers [44]. It has been observed that the type of conductivity depends on sulfur concentration. Conductivity type was tested from Hall measurements and confirmed by hot probe method. It is noted that the films grown at

Table 5 Electrical Properties of SnS2 films deposited at various sulfur concentration

Sulfur molar concentration (M)	Resistivity (ohm-cm) $\times 10^2$	Conductivity (1/ohm-cm) $\times 10^{-3}$	Carrier concentration (/cm³)	Mobility (cm²/V s) $\times 10^2$	Type of conductivity
0.8	6.09	1.63	6.94×10^{13}	1.47	P
0.9	1.84	5.43	4.09×10^{13}	8.27	N
1.0	0.11	99.3	2.05×10^{15}	3.01	N

1.0 and 0.9 M of sulfur concentration showed n-type conductivity. However, the films prepared with 0.8 M of sulfur concentration exhibited p-type conductivity. It might be due to the variation of stoichiometry of the films with 0.8 M concentration (Sn/S ratio is shown in Fig. 6) [32, 45]. Hence, the films were prepared, using the optimized concentration (0.9 and 1.0 M) of sulfur to obtain single phase n-type SnS_2 films which can be used as window layer in solar cells. This observation confirmed that conductivity type of SnS_2 films can essentially be controlled by sulfur concentration. Hence, homo-junction can be easily formed by sequential deposition of n and p-type SnS_2 layers using different sulfur concentration at same substrate temperature (T_s) in NSP technique [32].

5 Conclusion

SnS_2 thin films were coated using nebulizer spray pyrolysis technique by varying sulfur concentration. Improvement in structural and morphological properties of SnS_2 thin film was inferred by changing the sulfur concentration. XRD study confirmed the hexagonal phase crystalline growth of SnS_2 thin films with (002) plane preferred orientation. Concentration variation is also found to tune the morphology of the films, different morphologies like sheets and rods have been obtained. EDAX study showed linear increase of atomic percentage of sulfur in the films for the change of precursor concentration from 0.8 to 1.0 M. Optical characterization showed a band gap variation from 2.15 to 2.01 eV for sulfur concentration from 1.0 to 0.8 M, respectively. Sulfur concentration of 1.0 M has shown high transmittance compared to other concentrations. Minimum electrical resistivity about 11 Ω.cm was obtained for SnS_2 thin films prepared at 1.0 M concentration. It could be inferred from this work that 1.0 M of sulfur concentration can yield superior quality SnS_2 thin film useful for solar cell and photo detector applications.

References

1. M. Messaoudi, M.S. Aida, N. Attaf, T. Bezzi, J. Bougdira, G. Medjahdi, Mater. Sci. Semicond. Process **17**, 38–42 (2014)
2. R.K. Ramakrishna, R.N. Koteswara, R.W. Miles, Sol. Energy Mater. Sol. Cells **90**, 3041 (2006)
3. N.G. Deshpande, A.A. Sagade, Y.G. Gudage, C.D. Lokhande, R. Sharma, J. Alloys Compd. **436**, 421–426 (2007)
4. A.Y. Jaber, S.N. Alamri, M.S. Aida, Jpn. J. Appl. Phys. **51**, 065801 (2012)
5. I.B. Kherchachi, H. Saidi, A. Attaf, N. Attaf, A. Bouhdjar, H. Bendjdidi, Y. Benkhetta, R. Azizi, M. Jlassi, Optik **127**, 4043–4046 (2016)
6. R.D. Engelken, H.E. Mc Cloud, C. Lee, M. Slayton, J. Electrochem. Soc. **134**, 2696 (1987)
7. S. Acharya, O.N. Srivastava, Electronic Behavior of SnS_2 crystals. J. Phys. Status Solidi **65**, 717–723 (1981)
8. I.B. Kherchachi, A. Attaf, H. Saidi, A. Bouhdjer, H. Bendjedidi, Y. Benkhetta, R. Azizi, Structural optical and electrical properties of Sn×S y thin films grown by spray ultrasonic. J. Semicond. **37**, (2016)
9. K. Matsumoto, S. Kaneko, Thin Solid Films **121**, 227 (1984)
10. J. Li, Y.C. Zhang, M. Zhang, Mater. Sci. Forum **663–665**, 104–107 (2011)
11. S. Lopez, A. Ortiz, Semicond. Sci. Technol. **9**, 2130–22133 (1994)
12. T. Shibata, T. Miura, T. Kishi, T. Nagai, J. Cryst. Growth **106**, 593–604 (1990)
13. B. Ghosh, M. Das, P. Banerjee, S. Das, Appl. Surf. Sci. **254**, 6436 (2008)
14. A. Tanusevski, D. Poelman, Sol. Energy Mater. Sol. Cells **80**, 297 (2003)
15. M. Ichimura, K. Takeuchi, Y. Ono, E. Arai, Thin Solid Films **361–362**, 98–101 (2000)
16. M. Patel, I. Mukhopadhyay, A. Ray, Opt. Mater. **35**, 1693–1699 (2013)
17. N. Sethupathi, P. Thirunavukkarasu, V.S. Vidhya, R. Thangamuthu, G.V.M. Kiruthika, K. Perumal, H.C. Bajaj, M. Jayachandran, J. Mater. Sci. **23**, 1087–1093 (2012)
18. S.K. Panda, A. Antonakos, E. Liarokapis, S. Bhattacharya, S. Chaudhuri, Mater. Res. Bull. **42**, 576–583 (2007)
19. K. Vijayakumar, C. Sanjeeviraja, M. Jayachandran, L. Amalraja, J. Mater. Sci. **22**, 929–935 (2011)
20. A.D. Pogrebnjak, T.O. Berestok, A.S. Opanasyuk, Y. Takeda, K. Oyoshi, F.F. Komarov, J. Nano- Electron. Phys. **6**, 1–5 (2014)
21. A. Voznyi, V. Kosyak, A. Opanasyuk, N. Tirkusova, L. Grase, A. Medvids, G. Mezinskis, Mater. Chem. Phys. **173**, 1–10 (2016)
22. A.S. Opanasyuk, D.I. Kurbatov, V.V. Kosyak, S.I. Kshniakina, S.N. Danilchenko, Crystallogr. Rep. **57**, 927–933 (2012)
23. V.G. Hadjiev, D. De, H.B. Peng, J. Manongdo, A.M. Guloy, Phys. Rev. B **87**, 104302 (2013)
24. J.S. Cruz, K. Monfil Leyva, N.R. Mathews, A. Mendoza Galvan, X. Mathew, Chalcogenide Lett. **12**, 415–427 (2015)
25. C.-H. Hsu, L.-C. Chen, X. Zhang, Materials **7**, 1261–1270 (2014)
26. C.D. Lokhande, J. Phys. D **23**, 1703 (1990)
27. K.L. Chopra, *Thin Film Phenomena*. (McGraw-Hill, New York, 1969), p. 270
28. G. Lucovsky, J.C.J. Mikkelson, W.Y. Liang, R.M. White, R.M. Martin, Phys. Rev. B **14**, 1663 (1976)
29. A. Mukherjee, P. Mitra, Mater. Sci.-Pol. **33**(4), 847–851 (2015)
30. P. Mani, K. Manikandan, J.J. Prince, J. Mater. Sci. **27**, 9255–9264 (2016)
31. K. Manikandan, P. Mani, C.S. Dilip, S. Valli, P.F.H. Inbaraj, J.J. Prince, Appl. Surf. Sci. **288**, 76–82 (2014)
32. T.H. Sajeesh, R. Anita, C.S. Kartha, K.P. Vijayakumar, Thin Solid Films **518**, 4370–4374 (2010)
33. S. Polivtseva, I. Oja Acik, A. Katerski, A. Mere, V. Mikli, M. Krunks, Energy Procedia **60**, 156–165 (2014)
34. T. Rath, L. Gury, I. Sanchez-Molina, L. Martinez, S.A. Haque, R. Soc. Chem. **51**, (2015)
35. T. Sall, B. Mari, M. Mollar, J. Mater. Sci. **51**, 7607–7613 (2016)
36. V. An, M. Dronova, A. Zakharov, Chalcogenide Lett. **12**, 483–487 (2015)
37. A. Mukherjee, P. Mitra, Indian J. Phys. **89**, 1007–1012 (2015)
38. O.A. Yassin, A.A. Abdelaziz, A.Y. Jaber, Mater. Sci. Semicond. Process. **38**, 81–86 (2015)

39. N.K. Abass, A.A. Baker, A.J. Cadhum, N.A. Mahmood, Baghdad Sci. J. **7** (2010)
40. B.A. Hasan, I.H. Shallal, J. Nanotechnol. Adv. Mater. **2**, 43–49 (2014)
41. M. Salavati-Niasari, M.R. Loghman-Estarki, F. Davar, Inorg. Chim. Acta **362**, 3677–3683 (2009)
42. G. Kiruthigaa, C. Manoharan, M. Bououdina, S. Ramalingam, C. Raju, Solid State Sci. **44**, 32–38 (2015)
43. G. Ham, S. Shin, J. Park, J. Lee, H. Choi, S. Lee, H. Jeon, RSC Adv. **6**, 54069–54075 (2016)
44. N.K. Reddy, K.T.R. Reddy, Solid-State Electron. **49**, 902–906 (2005)
45. N.K. Reddy, K.T.R. Reddy, G. Fisher, R. Best, P.K. Dutta, J Phys D **32**, 988–990 (1999)